

## Research Article

## Laser Welding for Dissimilar Metals Stainless Steel AISI 304H, to Low Carbon Steel DIN St33, by Nd: YAG Laser

Jassim M. Salman<sup>A\*</sup> and Khalid Mutashar Abed<sup>A</sup><sup>A</sup>University of Babylon, College of Matrial Engineering, Iraq

Accepted 01 Oct 2014, Available online 10 Oct 2014, Vol.4, No.5 (Oct 2014)

### Abstract

In this research dissimilar welds were made of low carbon steel (DIN St33) 0.5 mm thickness and austenitic stainless steel (304H) 0.5 mm thickness by Nd: YAG laser beam welding (LBW). The effect of laser parameters (i.e peak power and welding speed) on joint strength, microhardness and microstructure has been investigated experimentally. Five level of peak power 5, 5.5, 6, 6.5 and 7 kW respectively, were varied (keeping constant pulse duration 4.7 ms, pulse repetition rate 1.5 Hz and welding speed 0.5 mm/sec). For the effect of welding speed five levels of welding speed 0.3, 0.8, 1, 1.3, and 1.5 mm/sec respectively, were varied (keeping constant peak power 5.5 kW, pulse duration 5.2 ms and pulse repetition rate 2.8 Hz). The experimental investigation included, tensile shear test, microhardness, microstructure and EDS analysis. It was found that the best welding condition, for maximum joint strength (408N), is 6.5 peak power, it was found for the effect of welding speed, that the best welding condition, for maximum joint strength (433N) is 1 mm/sec. Hardness tests showed that the highest hardness value appears in (WZ).

**Keywords:** Austenitic Stainless Steel (AISI 304H), Low carbon steel DIN St33, Nd: YAG lase , Dissimilar welds , Microstructure , Mechanical Properties.

### Introduction

Welding is generally defined as the process of thermally joining two materials. Depending upon the combination of temperature and pressure, a wide range of welding processes, like-gas welding, arc welding, resistance welding, solid state welding, thermo-chemical welding and high energy beam welding, have been developed. All these welding processes result different weld bead profiles, angular distortions and weld quality to weld-pieces as governed by the inherent characteristics of the process and processing parameters. Among the various welding processes, high energy beam welding employing laser has key benefits in terms of localized heating, faster cooling rate, smaller heat affected zone, and easier access that lead to reduced work piece distortion. It is widely employed for welding of metals, dissimilar materials, ceramics and polymers with various thicknesses and precision (L. Quintino *et al*, 2007; K. Kinoshita *et al*, 2006; A. Salminen *et al*, 2010; Y. Kawahito *et al*, 2007; J. Canning, 2006; K. Hafeez and S. Katayama, 2009).

Laser material processing is non-contact, flexible and accurate process applicable to a wide range of materials, and it is in rapid developing (Y. Yao, 2000). In laser welding, the process does not need very high intensity level and not having the minimum spot size (F. R. John, 1997). Welding is of particular interest in the automotive industry, joining steel body panels, transmission

components and chassis members during production (J. Zhou *et al*, 2006).

The use of laser for the manufacturing sector has unique advantages over the conventional means of welding due to high productivity, non-contact treatment, disposal of finishing operations, adaptability to automation, reducing the cost of treatment, improving product quality, and more use of equipment (J. Zhou *et al*, 2006).

### Materials Used

The selected metals to be joined using pulsed Nd:YAG laser for this work, are austenitic stainless steel AISI 304H and low carbon steel DIN St33. It is commonly found in the oil refining, gas and chemical industry and is used in industrial boilers, pressure vessels, heat exchangers, pipe lines and condensers. The material is also used throughout the power generation industry. It is versatile, general purpose stainless steel with good resistance to atmospheric corrosion, too many organic and inorganic chemicals, and to foods and beverages (Weman, 2003).

### Specifications

Chemical composition of the metals being used in the present work, was analyzed by using spectrometer type (Spectromax / Materials Analysis Division / Alloys; Fe, Ni, Cu, Al / Germany), at the State Company for Inspection and Engineering Rehabilitation (SIER).

\*Corresponding author: Dr. Jassim M. Salman

The obtained results were compared with the standards for assigning their grades. The chemical compositions of the selected metals are listed in Table (1). The mechanical properties for the selected metals are presented in Table (2) (Weman, 2003).

**Table 1** Chemical compositions of the metals used in Wt%

Element	Steel 304H	ST33 - 1.0035
C	0.092	0.088
Si	0.266	0.023
Mn	0.55	0.336
P	0.021	0.022
S	0.022	0.023
Cr	19.76	0.027
Mo	0.187	0.002
Ni	7.83	0.029
Al	0.004	0.012
Co	0.030	0.001
Cu	0.116	0.031
V	0.040	0.0005
Fe	Bal.	Bal.

**Table 2** Mechanical properties of the materials used

Property	Steel 304H	St33(1.0035)
Yield Stress (MPa)	205	185
Ultimate Stress (MPa)	515	310
Hardness (HRB)	92	60

**Specimen Preparation and Joint Design**

Several preparation steps were followed for both steel metal sheets specimens, AISI 304H stainless steel of 0.5mm thickness and DIN St33 low carbon steel of 0.5mm thickness. Those metals were cut to small plates of 100mm length and 20mm width and the overlap between each two pair of welded samples was 20mm. The stainless steel sheet was placed above the low carbon steel sheet as shown in Figure (1).

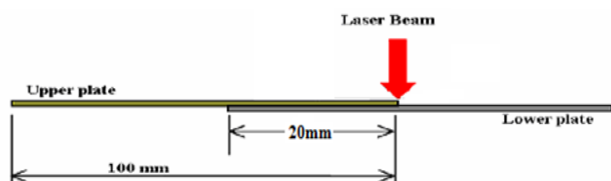


**Figure 1:** Schematic diagram illustrating the center-line welding lap-join

The edges of all plates were polished using different abrasive silicon carbide papers to attain a smooth surface finish. Noticeable care was taken to ensure the parallelism of the edges to each other and achieving no gap between them.

**Tensile Shear Test Results**

The tensile shear test for the laser welded lap joint was conducted at room temperature using (Universal Testing

Machine/Computer Control Electronic/ Model W.D.W. 200, Max. Load 200kN). The maximum withstand load of each weld joint was measured using a cross head speed of 10mm/min. The tensile tests showed that the fracture occurred outside the weld’s region (at HAZ), which means the weld’s region had a higher tensile strength than the base metal. The tensile test results displayed in the present work have been taken at the weld joint as shown in Figure (2).



**Figure 2:** Failure across tensile shear testing load

The experimental welding conditions and tensile shear testing results are presented in Tables (3,4).

**Effect of Peak Power**

Table (3) shows that sample no.4/group1 achieved maximum value for the shear force of 408N. The ultimate tensile strength of the welded joints increased gradually at the beginning and then decreased as the peak power increased. The penetration depth increased sharply by increasing the laser power. Peak power has a less influence on both weld profile and heat affected zone’s width in comparison with its effect on the penetration depth (T. Zacharia *et al*, 1989). The optimum power for full penetration with an acceptable weld profile (that is homogenous, without cracks, no cavities, etc.) was 6.5kW. The increase in peak power produces higher heat input which increase the target temperature producing steeper thermal gradients and severe thermal straining.

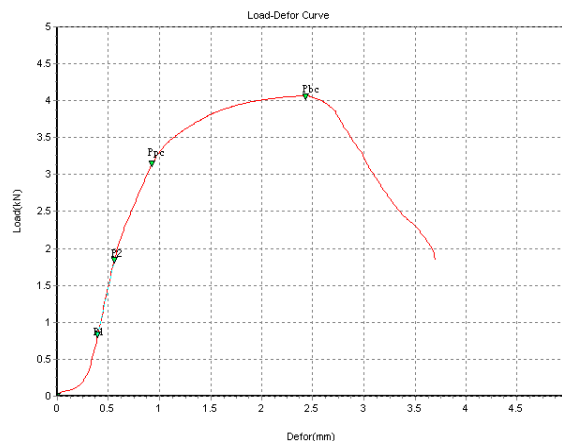


**Figure 3:** Sample no.4, P<sub>p</sub> of 6.5 kW

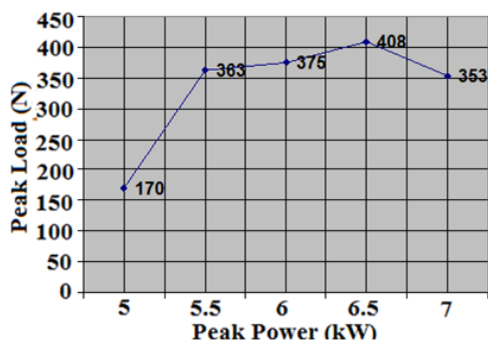
Load v/s displacement curves were plotted for each specimen. Figure 3 shows the results of specimen No 4.

**Table 3** Working parameters for samples of group one

Group No.	Sample No.	P <sub>p</sub> (kW)	Δt <sub>1/2</sub> (msec)	PRR Hz	Welding speed (mm/sec)	Shear Force (N)
G1	1	5	4.7	1.5	0.5	170
	2	5.5	4.7	1.5	0.5	363
	3	6	4.7	1.5	0.5	375
	4	6.5	4.7	1.5	0.5	408
	5	7	4.7	1.5	0.5	353

**Table 4** Working parameters for samples of group four

Group No.	Sample No.	P <sub>p</sub> (kW)	Δt <sub>1/2</sub> (msec)	PRR Hz	Welding Speed (mm/sec)	Shear Force (kN)
G4	1	5.5	5.2	2.8	0.3	347
	2	5.5	5.2	2.8	0.8	425
	3	5.5	5.2	2.8	1	433
	4	5.5	5.2	2.8	1.3	417
	5	5.5	5.2	2.8	1.5	413



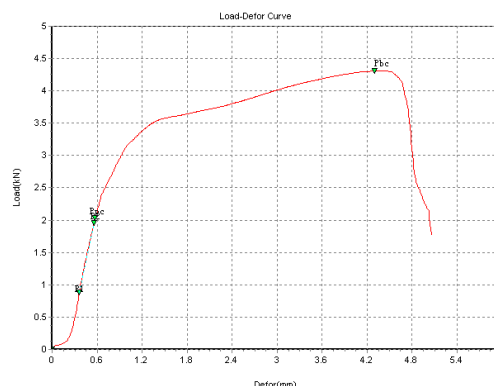
**Figure 4:** Peak load versus peak power at fixed Δt<sub>1/2</sub>, PRR, and W.S

Figure 3 shows that peak load increased by increasing the peak power. After attaining an optimum peak value the peak load decreased as the peak power increased. For this optimum value, the power is just sufficient to cause full penetration of the weld bead and forming a uniform weld region having good strength. Any levels less than this value will not have enough power to cause full penetration of the weld bead and produces weak joint. While at peak power higher than the optimum value, excessive power causes burn through the weld region. The joint gets weakened in the middle leading to a lower peak load. In this case peak power of 6.5kW was found to be the optimum value.

**Effect of Welding Speed**

Table 4 shows that sample No.3/group2 achieved maximum value for the shear force of 433N. The effect of welding speed was investigated at the optimum laser power of 5.5kW, pulse duration of 5.2msec, pulse repetition rate of 2.8 Hz, and 1mm/sec of welding speed. The depth/width ratio increased sharply by increasing the welding speed. A slower welding speed resulted in a considerable increase in the fusion zone size and consequently a decrease in depth/width ratio leading to unacceptable quality of weld profile. The following results show that the laser power and welding speed should be optimized in order to minimize the heat input and then a

satisfactory weld with reliable quality could be obtained. Load v/s displacement curve of each specimen was plotted as shown in Figure 3.



**Figure 4:** Sample no.3, W.S. of 1mm/sec

Figure 5 shows that peak load increases gradually by increasing welding speed. After attaining a maximum value of peak load the strength of the joint decreases as the welding speed decreases also. Higher welding speeds produce weak weld line due to the insufficient heat input because of the insufficient interaction time.

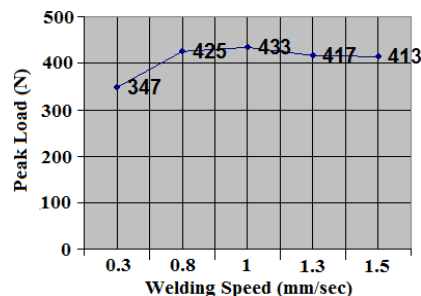


**Figure 5:** Peak Load versus welding speed at fixed P<sub>p</sub>, Δt<sub>1/2</sub>, and PRR

In other words, before the metals to be fully joined the laser beam moves to a new position. At very slow welding speeds an inverse case occurs due to the high heat input as the interaction time will be as long as enough to

evaporates the weld pool. Therefore, an optimum welding speed at which the highest tensile strength of the joint is to be achieved and it was found to be 1mm/sec as shown above.

The apparent shapes of the most successful sample of each group that shows the highest breaking force are shown in Figure 5. Sample G1/4 and G2/3 is the best of these four optimal samples.

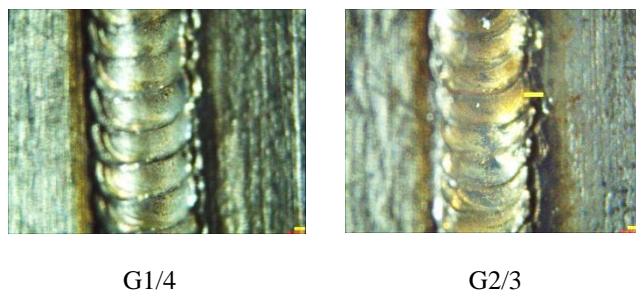


Figure 6: Apparent shapes of the most successful samples

**Microhardness**

The applied heat during welding process alters the microhardness of the material adjacent to the weld region. Hardness tests were performed to evaluate the hardness distribution across the weld line, the base material, and HAZ on both sides of the weld region (left and right).. The results show that the hardness of the weld zone is slightly higher than that for both HAZ and base metal because of recrystallization of finer grain size and dislocation density of the nugget during laser welding. Unsymmetrical microhardness profile can be pointed out. The center of the weld line achieved maximum hardness due to its rapid cooling rate.

High cooling rates create martensitic phase at the weld zone (S. Sundaresan and R. Janaki,1999). As the heat input increases the diffusion of Chromium, Nickel, and Carbon from parent metal towards weld interface can be noticed (A. Zambon et al, 2006; Ghaini et al, 2007).

**Effect of Peak Power**

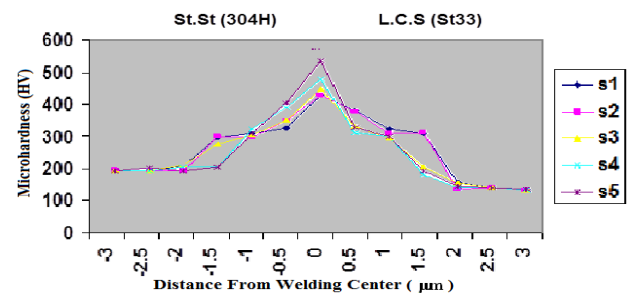


Figure 7: Micro-hardness distribution of workpiece for variant P<sub>p</sub> at fixed  $\Delta t_{1/2}$ , PRR, and W.S

It is observed that the hardness of dissimilar welds at the weld region is higher than that at HAZ and base metal from both sides of 304H and St.33. The hardness decreased slightly at different rates towards the base metal. Higher peak power density of laser beam welding provides

higher heat input and more rapid solidification when compared to the conventional techniques leading to higher hardness values. At HAZ, heating arises from the weld pool so the hardness is lower than the weld pool.

The locations (as a distance from the welding center) at which the micro-hardness was measured were presented in Figure 7.

Figure 8 shows the relation between various peak powers of (5, 5.5, 6, 6.5, and 7) kW and micro-hardness at fixed pulse duration of 5msec, pulse repetition rate of 1.5Hz, and welding speed of 0.5mm/sec.

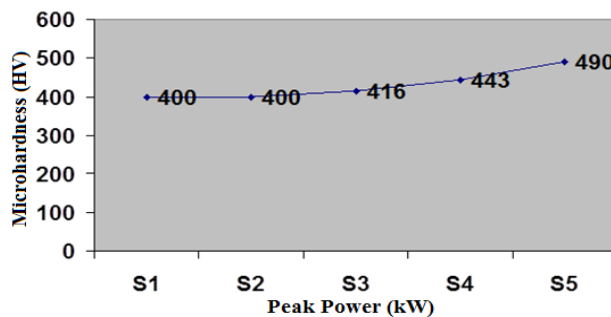


Figure 8: Micro-hardness at fusion pool for different P<sub>p</sub> levels.

**Effect of Welding Speed**

The heat input is decreased by increasing the welding speed because of no sufficient interaction time between the laser beam and the workpiece leading to creating lower temperature gradient between the workpiece and the surrounding which result lower cooling rate which is not adequate for achieving high hardness levels. And because of that the width of the weld line and the HAZ are decreased also. Micro-hardness decreases by increasing the welding speed. The best welding speed that achieved highest breaking force at fixed peak power of 5.5kW, pulse repetition rate of 2.8Hz, and pulse duration of 5.2msec is that for sample G2/3 which was 1mm/sec.

The locations (as a distance from the welding center) at which the micro-hardness was measured were presented in Figure 9.

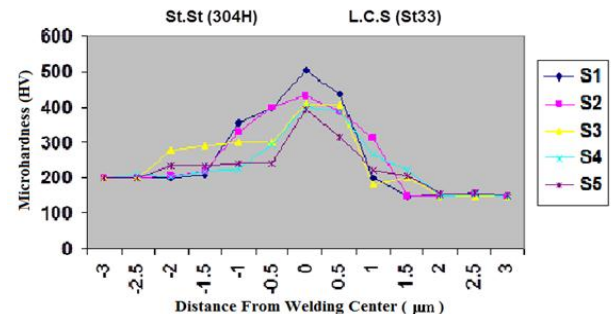
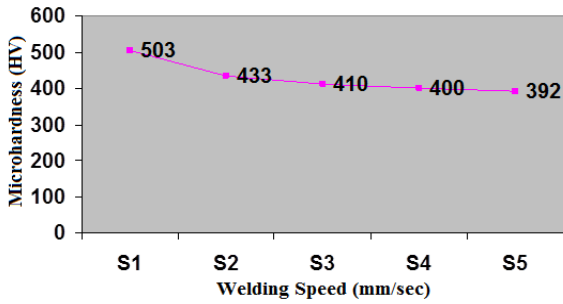


Figure 9: Micro-hardness distribution of workpiece for variant W.S. at fixed P<sub>p</sub>,  $\Delta t_{1/2}$ , and PRR

Figure 10 shows the relation of various welding speeds (0.3, 0.8, 1, 1.3, and 1.5) mm/sec versus micro-hardness at fixed peak power of 5.5kW, pulse duration of 5.2msec, and pulse repetition rate of 2.8Hz.



**Figure 10:** Micro-hardness at fusion pool for different W.S. levels

**Microstructure**

The fusion area (also known as the weld metal), the HAZ, and the unaffected base metal (BM) are three distinct regions for the welding process. Analyzing the microstructure for the optimal parameters shows that the shape of the fusion zone is regular and symmetric and the width of the HAZ is very narrow. At the welded zone, austenite cellular dendrite structure grows from fusion boundary to the center of the molten metal. A dendritic microstructure was developed at fusion boundary due to fast cooling conditions as in Figure 11,12 (e). At HAZ grain size is significantly smaller than the grain size of the base metal because during laser welding the material melts in a very short period and solidified quickly which leads to the difference between the microstructure due to laser welding and that of the conventional welding methods. Delta ferrite which is contrasted as dark holes is slightly observed on the boundary of primary precipitated austenite cell (B. Yilbas *et al*, 1998). Figure 11 (a, b, c, and e) shows the microstructure of dissimilar welding of stainless steel (304H) and low carbon steel (St33) represented by sample G1/4 and G2/3. It shows that the welded zone at the interface between the two joined metals has different microstructure (T. Zacharia *et al*, 1989). The microstructures of all types of laser beam welding are always austenitic with a few percent of delta-ferrite at the dendrite boundaries (A. Schaeffler, 1949). This achieved best effect on reducing the probability of forming micro-cracks at the weld zone. The reason for that is  $\delta$  Ferrite phase dissolves harmful elements like Sulfur and Phosphorous which contribute to form micro-cracks at the weld zone (J. Brooks and J. Williams, 1984; V. Kujanpaa, 1984).

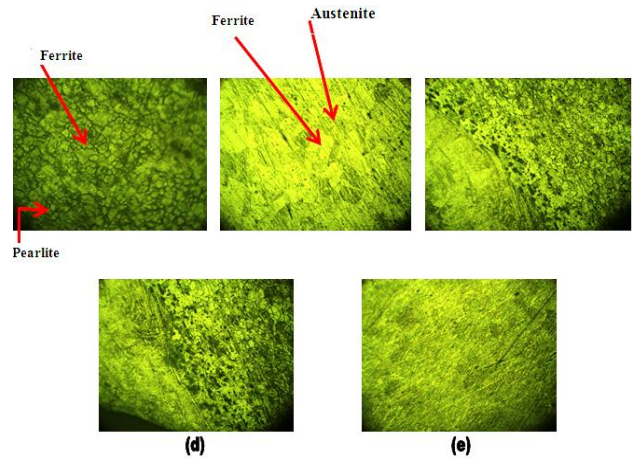
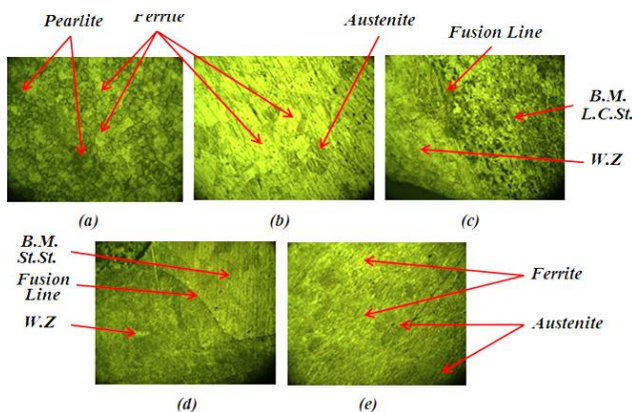
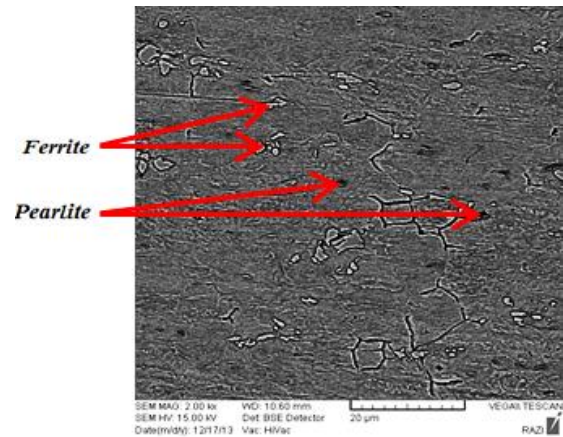


**Figure 11:** The microstructure of sample G1/4, (a); B.M. (L.C.St), (b); B.M. (St.St.), (c); HAZ (L.C.St.), (d); HAZ (St.St.), (e); W.M. (L.C.St. & St.St.)

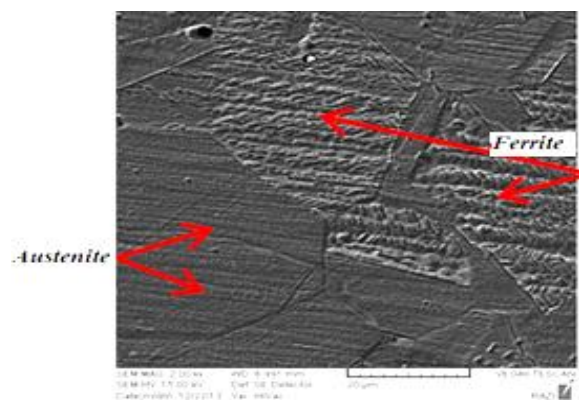
Figure 11 (a, b, c, d, and e) shows the microstructure of the optimum sample G1/4 that examined using scanning electron microscope (SEM).

Figure 12 (a, b, c, d, and e) shows the microstructure of the optimum sample G2/3 that examined using scanning electron microscope (SEM).

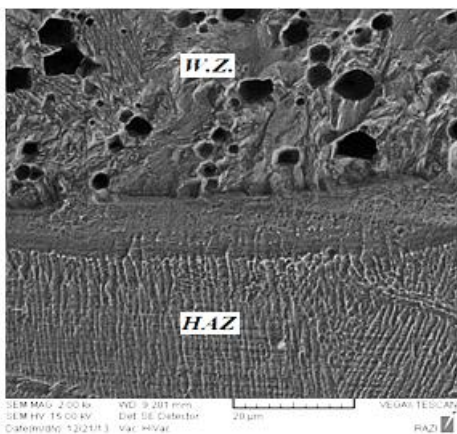
The SEM examination showed a very fine grained microstructure, which was basically dendritic in the weld region and this is variables for all parameters.



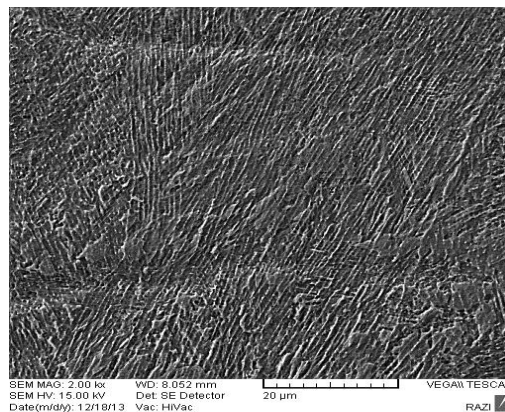
(a)



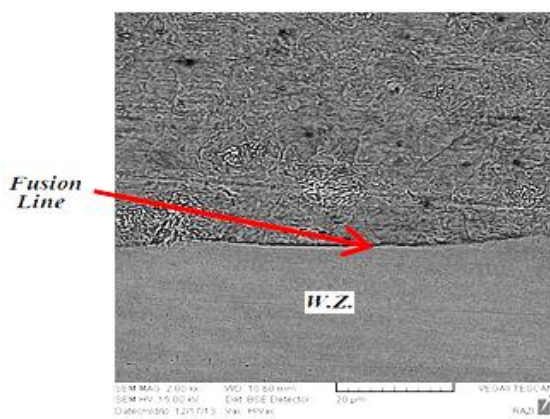
(b)



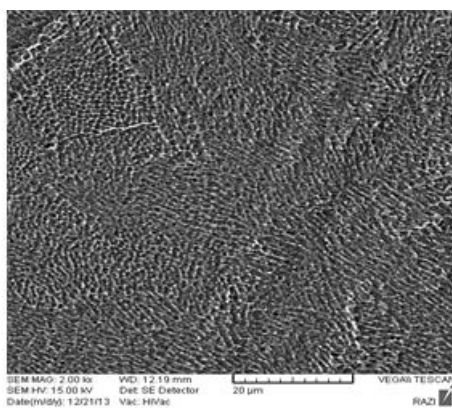
(c)



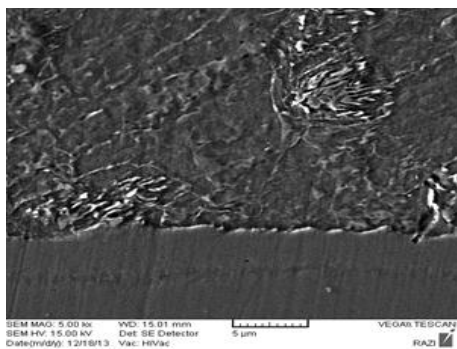
(g)



(d)



(e)



(f)

**Figure 12:** The microstructure of the optimum sample G2/3 using scanning electron microscope (SEM, (a); B.M. (L.C.St.), (b); B.M. (St.St.), (c); HAZ (L.C.St.), (d); HAZ (St.St.), (e); W.M. (Solidified structure of Austenitic and delta ferritic phases).

**Energy Dispersive X-ray Spectroscopy (EDS) Analysis**

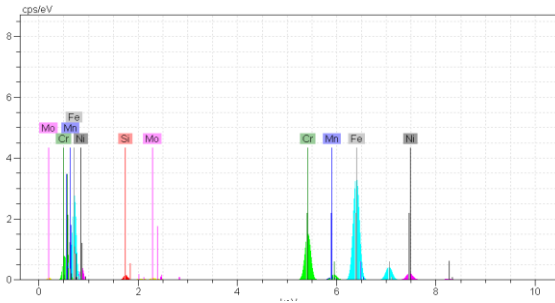
Peak power, and welding speed all have an important effect on heat flow and fluid flow during seam welding. These in turn affect the penetration depth, shape and final solidification structure of the fusion zone. Both shape and microstructure of the fusion zone are considerably influence the properties of the welding zone. The most successful sample of two groups which is G1/4 and G2/3 are examined by (EDS).

Long interaction period affects the diffusion of Cr, Ni, and other elements towards weld metal. At HAZ the chromium is depleted through formation of chromium carbide which precipitates at grain boundaries in the range of 425-475°C.

Peak power which controls the maximum power of each pulse affects the penetration depth and consequently affects the area of HAZ, welding area, and diffusion of Chromium, Nickel, and other alloying elements. As the welding speed is twice larger than the rest samples it is noticed that the diffusion of Chromium, Nickel, and other alloying elements at HAZ and welding region is decreased as the welding speed is increased. Consequently the area of the weld (width) and the HAZ are decreased by increasing welding speed due to less heat input at weld zone, high cooling rate, and short period for the alloying elements to diffuse (A. Sahin *et al*, 2010). Figure 13 (a, b, c, and d) shows all above mentioned effects graphically.

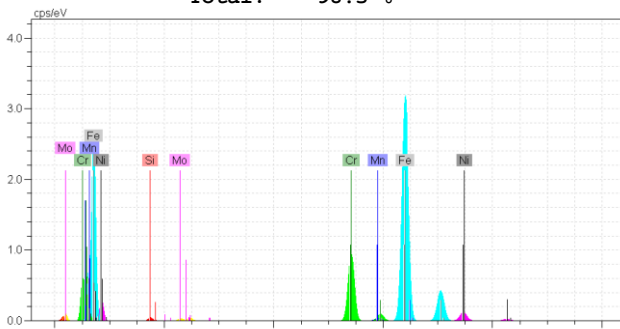
Spectra: Base Metal Stainless Steel G1/S4

Element	Series	unn. C [wt.-%]	norm. C [wt.-%]	Atom. C [at.-%]
Silicon	K series	0.47	0.48	0.95
Chromium	K series	16.24	16.56	17.58
Manganese	K series	1.19	1.22	1.22
Iron	K series	72.13	73.54	72.72
Nickel	K series	7.53	7.67	7.22
Molybdenum	L series	0.52	0.53	0.30
Total:		98.1	%	



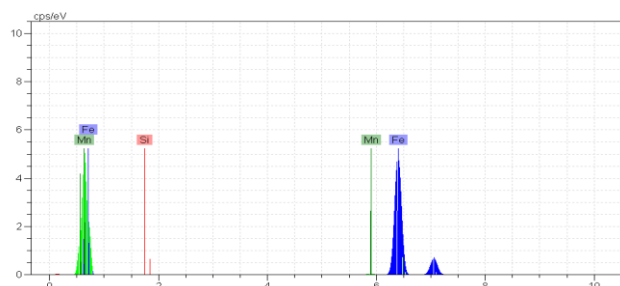
Spectra: HAZ-Stainless Steel G1/S4

Element	Series	unn. C [wt.-%]	norm. C [wt.-%]	Atom. C [at.-%]
Silicon	K series	0.17	0.18	0.35
Chromium	K series	11.38	11.57	12.35
Manganese	K series	0.50	0.51	0.51
Iron	K series	80.60	81.99	81.46
Nickel	K series	5.36	5.45	5.15
Molybdenum	L series	0.30	0.31	0.18
<b>Total:</b>		<b>98.3 %</b>		



Spectra: BASE METAL LOW CARBON G1/S4

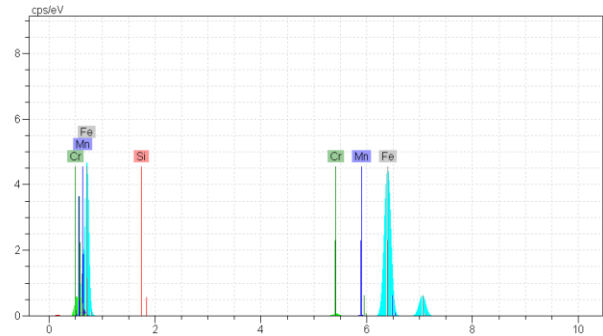
Element	Series	unn. C [wt.-%]	norm. C [wt.-%]	Atom. C [at.-%]
Silicon	K series	0.00	0.00	0.00
Manganese	K series	0.52	0.46	0.47
Iron	K series	112.42	99.53	99.53
<b>Total:</b>		<b>113.0 %</b>		



Spectrum

Spectra: HAZ-Low Carbon Steel G1/S4

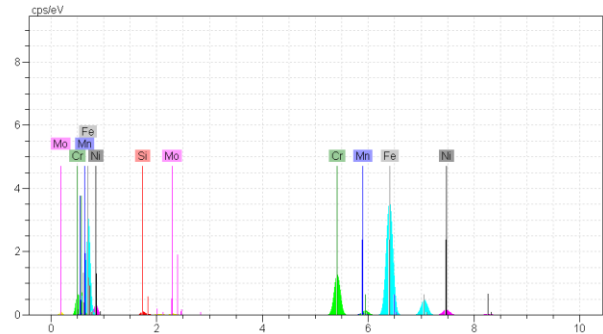
Element	Series	unn. C [wt.-%]	norm. C [wt.-%]	Atom. C [at.-%]
Silicon	K series	0.00	0.00	0.00
Chromium	K series	0.61	0.56	0.60
Manganese	K series	0.40	0.37	0.38
Iron	K series	107.36	99.07	99.02
<b>Total:</b>		<b>108.4 %</b>		



Spectrum

Spectra: WELDING AREA G1/S4

Element	Series	unn. C [wt.-%]	norm. C [wt.-%]	Atom. C [at.-%]
Silicon	K series	0.38	0.39	0.77
Chromium	K series	13.03	13.37	14.24
Manganese	K series	0.83	0.86	0.86
Iron	K series	76.63	78.66	77.98
Nickel	K series	6.03	6.19	5.84
Molybdenum	L series	0.51	0.53	0.30
<b>Total:</b>		<b>97.4 %</b>		

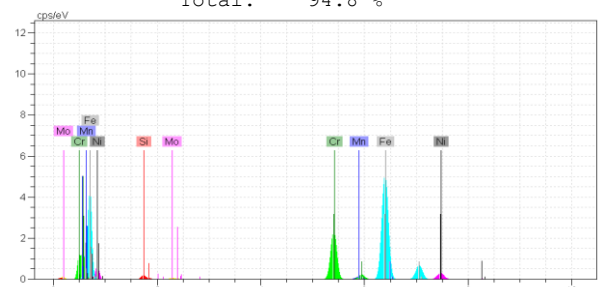


Spectrum

Figure 13 shows effects of peak power graphically.

Spectra: Base Metal-Stainless Steel G2/S3

Element	Series	unn. C [wt.-%]	norm. C [wt.-%]	Atom. C [at.-%]
Silicon	K series	0.49	0.52	1.02
Chromium	K series	16.26	17.16	18.18
Manganese	K series	1.16	1.23	1.23
Iron	K series	70.38	74.26	73.26
Nickel	K series	6.20	6.54	6.14
Molybdenum	L series	0.28	0.30	0.17
<b>Total:</b>		<b>94.8 %</b>		

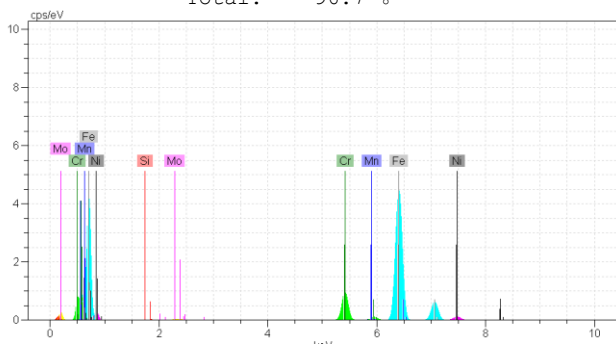


Spectrum

Spectra: HAZ-Stainless Steel G2/S3

Element	Series	unn. C [wt.-%]	norm. C [wt.-%]	Atom. C [at.-%]
Silicon	K series	0.04	0.05	0.09
Chromium	K series	8.08	8.35	8.93
Manganese	K series	0.46	0.48	0.48
Iron	K series	84.70	87.58	87.21
Nickel	K series	3.25	3.36	3.18
Molybdenum	L series	0.18	0.18	0.10

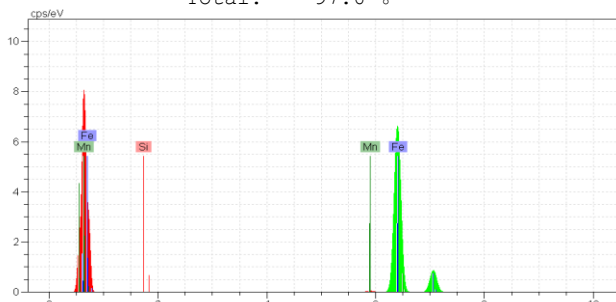
Total: 96.7 %



Spectra: Base Metal- Low Carbon Steel G2/S3

Element	Series	unn. C [wt.-%]	norm. C [wt.-%]	Atom. C [at.-%]
Silicon	K series	0.00	0.00	0.00
Manganese	K series	0.52	0.53	0.54
Iron	K series	97.11	99.47	99.46

Total: 97.6 %

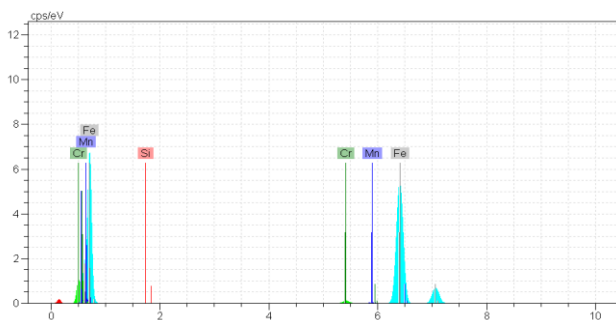


Spectrum

Spectra: HAZ/ Low Carbon Steel- G2/S3

Element	Series	unn. C [wt.-%]	norm. C [wt.-%]	Atom. C [at.-%]
Silicon	K series	0.00	0.00	0.00
Chromium	K series	0.81	0.83	0.90
Manganese	K series	0.36	0.38	0.38
Iron	K series	95.32	98.79	98.72

Total: 96.5 %



Spectra: WELDING AREA G2/S3

Element	Series	unn. C [wt.-%]	norm. C [wt.-%]	Atom. C [at.-%]
Silicon	K series	0.33	0.36	0.71
Chromium	K series	9.20	10.08	10.77
Manganese	K series	0.88	0.96	0.97
Iron	K series	76.45	83.78	83.29
Nickel	K series	3.67	4.02	3.80
Molybdenum	L series	0.73	0.80	0.46

Total: 91.3 %

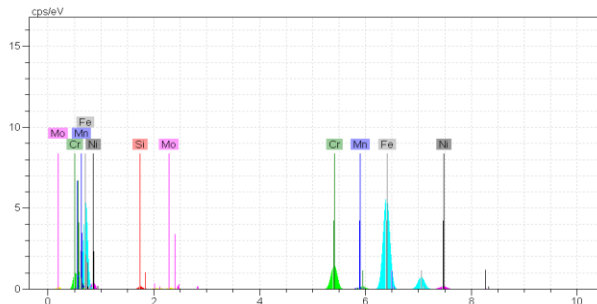


Figure 14 shows effects of welding speed graphically

Conclusions

In this study, tensile shear strength, micro-hardness, microstructural characteristics and EDS analysis of dissimilar welded (austenitic stainless steel AISI 304H, and low carbon steel DIN St33) via variable parameters (peak power, and welding speed) of laser beam welding (LBW) were analyzed. The obtained results were as following;

- 1- AISI 304H austenitic stainless steel is joined with St.33 low carbon steel by laser welding for two groups. The first group was executed at various peak powers of (5, 5.5, 6, 6.5, and 7) kW and fixed pulse duration of 5msec, pulse repetition rate of 1.5Hz, and welding speed of 0.5mm/sec. the two at various welding speeds of (0.3, 0.8, 1, 1.3, and 1.5) mm/sec and fixed peak power of 5.5kW, pulse duration of 5.2msec, and pulse repetition rate of 2.8Hz.
- 2- The optimal sample which is G2/3 was executed at peak power of 5.5kW, pulse duration of 5.8msec, pulse repetition rate of 1.5Hz, and welding speed of 1 mm/sec achieved maximum breaking force 433N at the weld zone and maximum hardness of 650 HV. This is due to high heat input and diffusion of chromium, Nickel, and carbon from the base metals towards the heat affected zones for both metals and fusion zone.
- 3- The best properties in terms of microstructure, micro-hardness, and tensile shear test were observed for sample G2/3.
- 4- The EDS analysis shows that diffusion of alloying elements of Chromium, Nickel, and other elements from base metals towards the heat affected zones for both metals and fusion zone are laser parameters dependent.

References

Quintino L., Costa A., Miranda R.,Yapp D., Kumar V, Kong CJ. (2007), Welding with High Power Fiber Lasers – A Preliminary Study, pp. 1231–7.

- Kinoshita K., Mizutani M., Kawahito Y., Katayama S. (2006), Phenomena of Welding with High-Power Fiber Laser, In: Congress proceedings of ICALEOs, Joining and Welding Research Institute, Osaka University, pp.535–41.
- Salminen A., Piili H., Purtonen T. (2010), The Characteristics of High Power Fiber Laser Welding, Proc I Mech. E Part C: J Mech. Eng. Sci 224.
- Kawahito Y., Mizutani M., Katayama S. (2007), Investigation of High Power Fiber Laser Welding Phenomena of Stainless Steel, Trans J WRI, 36 (2).
- Canning J. (2006), Fiber Lasers and Related Technologies, Opt. Lasers Eng. 44-64776.
- Hafeez K., Katayama S. (2000), Fiber Laser Welding of AISI304 Stainless Steel Plates, Trans J WRI, 27(2):63–73, 2009
- Yao Y., Introduction to the Laser Machining Process (Nontraditional-Manufacturing), Columbia University, National Science Foundation (CRCD EEC-98-13028), New York, USA.
- John F. R. (1997) Industrial Applications of Lasers, Second Edition, Academic Press, London.
- Zhou J., Hai L., Pei Chung W., Transport Phenomena and Keyhole Dynamics during Pulsed Laser Welding, Journal of Heat Transfer, Vol. 18, pp. 680-690, 2006.
- Weman (2003), Welding Processes Handbook, Woodhead Publishing Ltd..
- Zacharia T., David S., Vitek J., Debroy T. (1989), Welding Journal, 68, 12.
- Sundaresan S., Janaki R. (1999), Use of Magnetic Arc Oscillation for Grain Refinement of Gas Tungsten Arc Weld in Alpha-Beta Titanium Alloys, Science Technology, Weld join, 4, pp. 151-160.
- Zambon A., Ferro p., Bonollo F. (2006), Microstructural, Compositional and Residual Stress Evaluation of CO<sub>2</sub> Laser Welded Super Austenitic AISI 904L Stainless Steel, Materials Science and Engineering A, 424, pp. 117-127.
- Hamedi, Torkamany, Sabbaghzadeh (2007), Weld Metal Microstructural Characteristics in Pulsed Nd:YAG Laser Welding, Scripta Materialia, 56, pp. 955-958.
- Yilbas B., Sami M., Nickel J., Coban A., Said S. (1998), Introduction into The Electron Beam Welding of Austenitic 321-Type Stainless Steel, Journal of Materials Processing Technology, 82, pp. 13-20.
- Schaeffler A. (1949.), Metal proger, 5b, 680,
- Brooks J., Williams J. (1984), Fundamentals Study of the Beneficial Effects of  $\delta$  Ferrite in Reducing Weld Cracks, Welding Journal, Vol. 63, No. 6, pp. 715.
- Kujanpaa V. (1984), Weld Discontinuities in Austenitic Stainless Steel Sheet- Effect of Impurities and Solidification Mode, Welding Journal, Vol. 63, No. 12, pp. 369S-375S.
- Sahin A., Ayar T., Yilbas B. (2010), Laser Welding of Dissimilar Metals and Efficiency Analysis, Laser in Engineering.